Investigation of Non-equilibrium Radiation for Earth Entry

A. M. Brandis*†

AMA Inc. at NASA Ames Research Center, Mountain View, CA, 94035, USA,

C. O. Johnston*

NASA Langley Research Center, Hampton, VA, 23669, USA

B. A. Cruden‡

AMA Inc. at NASA Ames Research Center, Mountain View, CA, 94035, USA

For Earth re-entry at velocities between 8 and 11.5 km/s, the accuracy of NASA's computational fluid dynamic and radiative simulations of non-equilibrium shock layer radiation is assessed through comparisons with measurements. These measurements were obtained in NASA Ames Research Center's Electric Arc Shock Tube (EAST) facility. The experiments were aimed at measuring the spatially and spectrally resolved radiance at relevant entry conditions for both an approximate Earth atmosphere (79% N_2 : 21% O_2 by mole) as well as a more accurate composition featuring the trace species Ar and CO_2 (78.08% N_2 : 20.95% O_2 : 0.04% CO_2 : 0.93% Ar by mole). The experiments were configured to target a wide range of conditions, of which shots from 8 to 11.5 km/s at 0.2 Torr (26.7 Pa) are examined in this paper. The non-equilibrium component was chosen to be the focus of this study as it can account for a significant percentage of the emitted radiation for Earth re-entry, and more importantly, non-equilibrium has traditionally been assigned a large uncertainty for vehicle design. The main goals of this study are to present the shock tube data in the form of a non-equilibrium metric, evaluate the level of agreement between the experiment and simulations, identify key discrepancies and to examine critical aspects for accurately modeling non-equilibrium radiating flows. Radiance profiles integrated over discrete wavelength regions, ranging from the Vacuum Ultra Violet (VUV) through to the Near Infra-Red (NIR), were compared in order to maximize both the spectral coverage and the number of experiments that could be used in the analysis. A previously defined non-equilibrium metric has been used to allow comparisons with several shots and reveal trends in the data. Overall, LAURA/HARA is shown to under-predict EAST by as much as 40% and over-predict by as much as 12% depending on the shock speed. DPLR/NEQAIR is shown to under-predict EAST by as much as 50% and over-predict by as much as 20% depending on the shock speed. The one standard deviation scatter in the EAST results was calculated to be 31%. An estimate for the upper bound of the absolute error in wall-directed heat flux was calculated. Below 9 km/s, where the relative difference is large, the absolute error in radiative heat flux due to non-equilibrium models is estimated to be less than 1 W/cm^2. At the highest shock speed of 11 km/s, the error in non-equilibrium is estimated to be less than 20 W/cm^2.

I. Introduction

FUTURE Earth re-entry missions involving larger vehicles and higher entry velocities than previously encountered motivate the improved understanding of radiative heating and associated uncertainties. An example of such a mission is the next MPCV Orion flight, EM-1, which will undertake a lunar return trajectory where radiation will be a significant source of heating. Understanding these uncertainties may influence

*Senior Research Scientist, Aerothermodynamics Branch, and Senior Member AIAA.

†Contact: aaron.m.brandis@nasa.gov

‡Senior Research Scientist, Aerothermodynamics Branch, and Associate Fellow AIAA

future margin policies,[1] and hence the thermal protection system (TPS) material selection and thickness. A recent example of an attempt to better validate aerothermal calculations for flight is Exploration Flight Test 1 (EFT-1). EFT-1 entered Earth's atmosphere from a highly elliptical earth orbit in December of 2014. The heat shield of EFT-1 was instrumented (including radiometers) for the purposes of trajectory reconstruction and aerothermal model validation. At the velocity EFT-1 entered, radiative heating did not have a significant impact on either the total peak heat flux or heat load, but was significant enough to influence entry heating reconstruction. Since it is rare to have flight data available for verification and validation of the models implemented in computational tools, a detailed analysis to assess the level of agreement with state of the art simulations is warranted. Due to the trajectory flown by EFT-1, a significant portion of the radiative heat flux occurred at lower pressures and, as such, there was a large portion of non-equilibrium gas in the shock layer. Therefore, the present analysis attempts to provide insight into the accuracy of theoretical models in non-equilibrium by evaluating the level of agreement between flowfield/radiation simulations and data provided by EAST experiments.

Using shock tube data to validate non-equilibrium conditions should only be attempted if the characterization of equilibrium radiance is already well understood. Previous publications have focused on providing an extensive comparison between simulations and measurements of equilibrium radiation obtained in the EAST facility.[2,3] In these previous studies, the integrated value of equilibrium radiance was compared across several spectral regions as a function of velocity. Equilibrium becomes the dominant component of the radiation as velocity, free-stream density and shock stand-off distance increase. Results showed excellent agreement between HARA, NEQAIR and EAST data for the UV through IR spectral regions; however, discrepancies were identified in the VUV. As a result of this analysis, a parametric uncertainty for Earth re-entry above 10 km/s was evaluated to be [9.0%, -6.3%] $\pm$ 17%. For conditions below 10 km/s, it was concluded that the flow did not reach a sufficient level of equilibrium, and this was demonstrated via measurements of electron density in the "steady state" region of the flow in EAST being substantially larger than equilibrium predictions. The best current theory for this larger than equilibrium electron number density is due to the effect the deceleration of the shock has on the state of the gas. Since the shock deceleration is more prominent in the flow further behind the shock front, the assumption utilized in this work is that the gas directly behind the shock, i.e., the non-equilibrium region, is relatively unaffected.

II. Description of the EAST Facility

The EAST facility at NASA Ames Research Center was developed to simulate high-enthalpy, "real gas" phenomena encountered by hypersonic vehicles entering planetary atmospheres. EAST has the capability of producing super-orbital shock speeds using an electric arc driver with a driven tube diameter of 10.16 cm.[4,5] Experiments are performed to match flow parameters relevant to flight, such as velocity, static pressure, and atmospheric composition. The shock-heated test gas in the tube simulates conditions behind the bow shock of a re-entry vehicle. The region of valid test gas is located between the shock front and the contact surface that separates the driver and driven gases. The test duration is defined as the axial distance between these two points divided by the local shock velocity. The characteristics of the EAST arc driver result in test durations of approximately 4 - 10 μs. Though short, this test duration is often sufficient to capture the peak non-equilibrium shock radiation and the decay to equilibrium conditions. When the shocked gas arrives at the location of the test section in the tube, spectrometers attached to Charge Coupled Devices (CCDs) are gated, and the spectral and spatial emission of the gas are analyzed. EAST utilizes four spectrometers per shot, each associated with four different wavelength ranges. These cameras are referred to as: VUV ($\sim$ 120 – 215 nm), UV/Vis ($\sim$ 190 nm – 500 nm), Vis/NIR ($\sim$ 480 nm – 900 nm), and IR ($\sim$ 700 nm – 1650 nm).

III. Description of Simulation Tools

The non-equilibrium radiance results presented in this paper have been calculated from flowfield and radiation simulations, using two sets of codes, LAURA/HARA and DPLR/NEQAIR. This section will provide a brief overview of each software as well as detail some updates to the radiation codes relevant to this work. It is likely that further updates to all four codes will be motivated by the comparisons within this work and to the EFT-1 flight data.[6]

III.A. LAURA

The Langley Aerothermodynamic Upwind Relaxation Algorithm (Laura) is a structured grid flow solver, specialized for hypersonic re-entry physics, utilizing state-of-the-art algorithms for CFD simulations.[7,8] Fluxes are computed using Roe's averaging[9] and Yee's Symmetric Total Variation Diminishing (STVD)[10] formulation in order to obtain higher order accuracy.

III.B. HARA

The High-temperature Aerothermodynamic RAdiation (Hara) model applied in the present study is discussed in detail by Johnston et al.[11,12] A line-by-line approach is used for atoms and optically thick molecules, while a smeared band model is used for optically thin molecules. Hara is based on a set of atomic levels and lines from the National Institute of Standards and Technology (NIST)[13] and Opacity Project databases.[14] The atomic bound-free model is composed of cross sections from the Opacity project's online TOPbase,[15] which were curve fit by Johnston.[11] An update to the NO non-Boltzmann model in Hara has also been developed, as discussed in Johnston et al,[16] where non-Boltzmann rates were tuned to match EAST shock tube data from Ref. 2. This update to the NO non-Boltzmann model is not included in any of the Hara calculations presented in this paper unless it is specifically stated, as in section V.B. The analysis has been done this way, as predictions cannot be validated against data that it has been tuned to fit.

III.C. DPLR

Dplr[17–19] uses a finite-volume discretization to solve the reacting Navier-Stokes equations for fluids in thermochemical non-equilibrium on structured grids. While the software was originally designed for steady-state aerothermodynamic analysis of planetary entry vehicles, Dplr has evolved over the years to include a broad spectrum of numerical and physical models that enable it to accurately simulate most compressible flows. Additional details on Dplr's capabilities can be found in the references 17–19. The version of Dplr used in this work is the pre-release of v4.03.2. The new feature of this version relevant to this paper is the option allowing for the equivalence of vibration and electron/electronic energy, i.e. $T_v = T_e$. This paper provides a preliminary validation of the results provided by this updated energy coupling in Dplr.

III.D. NEQAIR

Non-EQuilibrium AIr Radiation (Neqair) is a line-by-line radiation code which computes spontaneous emission, absorption and stimulated emission due to transitions between various energy states of chemical species along a line-of-sight.[20] Individual electronic transitions are considered for atoms and molecules, with the molecular band systems being resolved for each rovibronic line. Since the report of Whiting et al.,[20] numerous updates have been incorporated into Neqair, such as: using the latest version of the NIST atomic database (version 5.0),[21] using the bound-free cross sections from TOPbase,[15] incorporating the CO_2 database from CDSD-4000,[22] parallelization and improvements to the mechanics of QSS. The current release version of Neqair is known as v14.0.[23]

The calculations in this paper use what will become the next release of Neqair, v15.0. This is due to Neqair v14.0 not including non-Boltzmann rates for states responsible for emission from N_2 2nd Positive, N_2 Birge-Hopfield 1 and high lying atomic lines. Therefore, a preliminary non-Boltzmann model[24,25] was introduced for the $C^3\Pi$ state of N_2 2nd Positive, while the states responsible for N_2 Birge-Hopfield 1 and atomic lines not included in non-Boltzmann were set to be in Boltzmann equilibrium (at T_e) with a state with the closest energy or orbital structure that is included in the non-Boltzmann model. Prior to these updates, recent versions of Neqair would subsequently treat these state populations as Boltzmann, resulting in large over-predictions of these bands and lines. These errors had been overlooked in previous studies since N_2 had not been a major contributor to radiative heating at lunar or hyperbolic return conditions. The electronic excitation rates for N atoms in Neqair have been updated to those of Huo.[26] This paper will show comparisons with the rates of Huo,[26] and the rates of Park[20] as implemented in v14.0.

IV. Methodology

IV.A. CFD Simulations

A two-dimensional grid of a 3 m sphere with 803 grid points on the stagnation line was used in the DPLR solutions, while a 2.5 m sphere with 256 points was used in the LAURA solutions. Both simulations used an 11-species (N_2, O_2, NO, NO^+, N_2^+, O_2^+, N, O, N^+, O^+, e^-) gas model in the computations. In addition to chemical non-equilibrium, the flow field was assumed to be in thermal non-equilibrium as well. Consequently, a two-temperature (T_{tr}-T_{ev}) model was used. In the two-temperature model employed, the translational and rotational modes of the molecules are assumed to be in equilibrium (T_{tr}=T_{trans}=T_{rot}), and are distinct from the vibrational and electronic modes of the molecules and the temperature of the free electrons (T_{ev} =T_{vib}=T_{elec}=T_{e^-}).

IV.B. Non-equilibrium Metrics

Insights into the agreement between simulations and experimental results have been made possible by analyzing integrated equilibrium spectra across a wide range of conditions and conducting detailed comparisons of the resulting trends.[2,3] For non-equilibrium flows, however, it is not immediately clear that one parameter can describe the level of non-equilibrium intensity observed in several shots over a large range of conditions. This is because the temporal intensity changes significantly with the shock speed as a result of the underlying change in the physics. The benefits and drawbacks of three proposed methods for determining a parameter that highlights either the relative significance of the non-equilibrium radiative intensity or the absolute intensity emitted in the non-equilibrium region was previously analyzed.[27] The goal of such a parameter is to enable the comparison of several simulations and experimental results while still maintaining a physically relevant meaning. Of these three methods, the absolute non-equilibrium metric is used in this work. This metric is computed by integrating the radiance within 2 cm of either side of the shock front, as shown by the red lines in Fig. 1, and is normalized by the shock tube diameter. Computing the metric in this manner has been suggested as a more robust way to conduct a comparison as opposed to using the peak intensity, since the comparisons are then not bound to experimental resolution limitations such as gate opening times and spatial smearing due to shock movement. Under optically thin conditions, this integral will represent the radiance as observed parallel to the direction of the shock. Under optically thick conditions, however, this integral is not physically meaningful and is simply a way of comparing data corresponding to a given optical path-length/shock tube diameter.

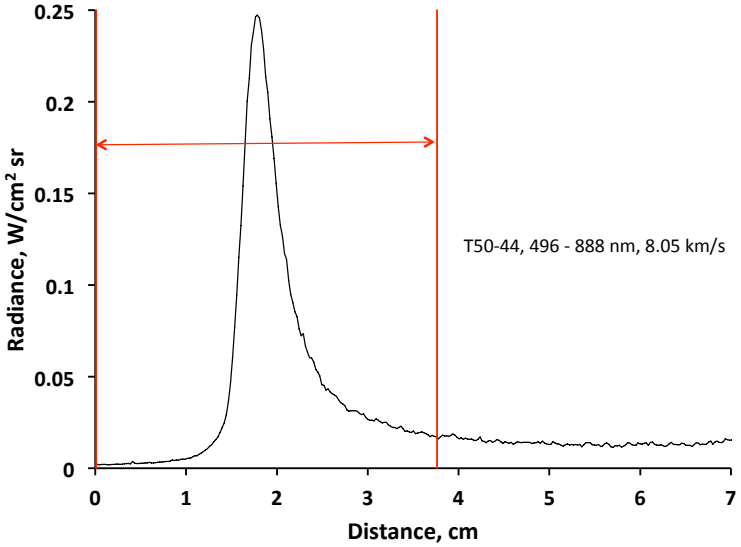

(a) Absolute non-equilibrium Radiance

Figure 1. Example of the "Absolute Metric" used in this work.

IV.C. Influence of Reaction Rates

Three different reaction rate sets used to simulate the non-equilibrium chemistry in the shocked flow have been examined in this analysis. The three chemical mechanisms include; the rates defined in Park 1990[28] and Park 1993,[29] as well as the rates included with the simulation tool LAURA.[16,30] In the following discussion, these models are referred to as the Park 90, Park 93, and LAURA reaction rate models. While the LAURA reaction rate set does utilize some of the heritage rates from both Park 90 and Park 93, more recent rates from a range of sources are also incorporated. The key differences between Park 90, Park 93 and the chemistry used in LAURA are detailed in Table 1.

The main difference between Park 90 and Park 93, is that Park 90 does not contain the nitrogen electron exchange reaction: $N^+ + N_2 \longleftrightarrow N_2^+ + N$. Since the chemical mechanism does not contain one of the most efficient pathways for N_2^+ to regain an electron through the electron exchange reaction, Park 90 results in excessive ionization predictions, as shown in Fig. 2(b). Figure 2(b) shows that the electron number density calculated with Park 90 is approximately 3 times higher than Park 93, and approximately 5 times higher than LAURA. This increased level of electrons causes the radiation calculation to provide excessive predictions. As such, comparisons between Park 90 simulations and EAST are made, but more detailed analyses computing the weighted radiance and the final overall summation of the differences between the simulations and EAST are not shown. It should also be noted that in the Park 90 reaction set used by DPLR, the electron impact ionization ($N + e \longleftrightarrow N^+ + 2e$) pre-exponential co-efficient is set to what is published in Park 93, as the Park 90 value is believed to be a typographical error.

An important difference between Park 90 / Park 93 and the chemistry used in LAURA is the NO dissociation rate. The tuning of the NO dissociation rate used in LAURA is deemed acceptable for validation because it is based on EAST data collected in a different mixture (CO_2/N_2), and measuring different molecular bands, than used here. It is hard to identify the effects of any one of the individual changes between the LAURA and Park chemistries; however, the net result can be seen in Fig. 2. Figure 2(a) shows that the translational temperature calculated by LAURA initially decays faster, then begins to relax slower than either of the Park models. The peak vibrational temperature calculated by LAURA is similar in magnitude to Park 90, both of which are slightly higher than that calculated with Park 93. The relaxation of the vibrational temperature in LAURA is significantly slower than both Park models. Figure 2(b) shows that the level of non-equilibrium overshoot in N, N^+ and e^- is significantly less when using LAURA compared to the Park models. This is not the case for N_2^+ and NO, which both show larger concentrations in the relaxation region with LAURA, as shown in Fig. 2(c).

Table 1. Key differences between the LAURA chemistry and the implementations of Park 90 and Park 93 in DPLR

i	Reaction	A_f $\mathrm{cm^3\ mole^{-1}\ s^{-1}}$	n_f	D_f K	T_f	T_r	Third Body, M
			Park 90				
1	$N^+ + N_2 \longleftrightarrow N_2^+ + N$				N/A		
2[28]	$NO + M \longleftrightarrow N + O + M$	1.1e+17	0	7.55e+4	$\sqrt{T_{tr}T_{ve}}$	T_{tr}	NO, N, O, N^+, O^+
		5.0e+15	0	7.55e+4	$\sqrt{T_{tr}T_{ve}}$	T_{tr}	N_2, O_2, NO^+, N_2^+, O_2^+
3[28]	$N_2 + e \longleftrightarrow N + N + e$	3.0e+24	-1.6	1.132e+5	$\sqrt{T_{tr}T_{ve}}$	T_{tr}	
4	$O_2 + e \longleftrightarrow O_2^+ + e + e$				N/A		
5[28]	$N_2 + O \longleftrightarrow NO + N$	6.4e+17	-1	3.84e+4	T_{tr}	T_{tr}	
6[28]	$NO + O \longleftrightarrow O_2 + N$	8.4e+12	0	1.945e+4	T_{tr}	T_{tr}	
			Park 93				
1[29]	$N^+ + N_2 \longleftrightarrow N_2^+ + N$	1.0e+12	0.5	1.22e+4	T_{tr}	T_{tr}	
2[28]	$NO + M \longleftrightarrow N + O + M$	1.1e+17	0	7.55e+4	$\sqrt{T_{tr}T_{ve}}$	T_{tr}	NO, N, O, N^+, O^+
		5.0e+15	0	7.55e+4	$\sqrt{T_{tr}T_{ve}}$	T_{tr}	N_2, O_2, NO^+, N_2^+, O_2^+
3[29]	$N_2 + e \longleftrightarrow N + N + e$	1.2e+25	-1.6	1.132e+5	$\sqrt{T_{tr}T_{ve}}$	T_{tr}	
4	$O_2 + e \longleftrightarrow O_2^+ + e + e$				N/A		
5[28]	$N_2 + O \longleftrightarrow NO + N$	6.4e+17	-1	3.84e+4	T_{tr}	T_{tr}	
6[28]	$NO + O \longleftrightarrow O_2 + N$	8.4e+12	0	1.945e+4	T_{tr}	T_{tr}	
			LAURA				
1[29]	$N^+ + N_2 \longleftrightarrow N_2^+ + N$	1.0e+12	0.5	1.22e+4	T_{tr}	T_{tr}	
2[16]	$NO + M \longleftrightarrow N + O + M$	4.4e+16	0	7.55e+4	$\sqrt{T_{tr}T_{ve}}$	T_{tr}	N, O, NO
		2.0e+15	0	7.55e+4	$\sqrt{T_{tr}T_{ve}}$	T_{tr}	others
3[31]	$N_2 + e \longleftrightarrow N + N + e$	6.0e+3	2.6	1.132e+5	T_{ve}	T_{ve}	
4[32]	$O_2 + e \longleftrightarrow O_2^+ + e + e$	2.19e+10	1.16	1.30e+5	T_{ve}	T_{ve}	
5[33]	$N_2 + O \longleftrightarrow NO + N$	6.0e+13	0.1	3.8e+4	T_{tr}	T_{tr}	
6[34]	$O_2 + N \longleftrightarrow NO + O$	2.49e+9	1.18	4.01e+3	T_{tr}	T_{tr}	

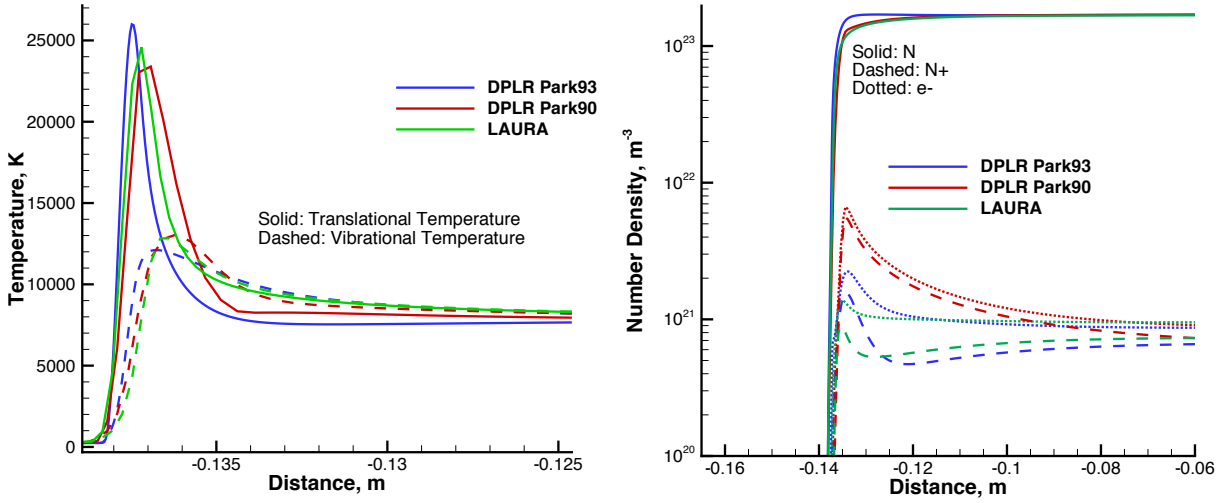

(a) Temperatures

(b) Number Densities of N, N^+ and e^-

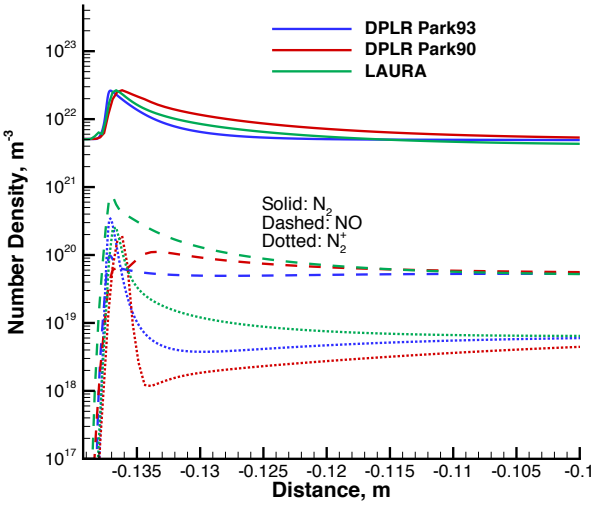

(c) Number Densities of N_2, NO, N_2^+

Figure 2. Flowfield comparison between different CFD solutions at 9 km/s and 0.2 Torr.

IV.D. Wavelength Regions Analyzed

The wavelength regions used in this analysis were picked to maximize the spectral coverage of the EAST data, see Table 2. The experimental results used in this study focus on EAST test campaigns 50[2,35] and 57 (this work). The radiation from these spectral regions is approximately 80 – 90% of the total radiative heat flux emitted. Regions containing a significant amount of carbon contamination, such as the 153 – 170 nm spectral region, have not been included in the analysis. While the 1445 – 1630 nm spectral range was measured in these tests, it contributes a negligible amount to the total radiative heat flux in the cases considered here ($< 0.1\%$), and is therefore excluded from the analysis. The percentage of the total radiation emitted as calculated by HARA from each of these wavelength regions based on the absolute non-equilibrium metric is shown in Fig. 3. The figure shows that at lower speeds (< 9.5 km/s) the radiance is dominated by molecular radiation emitted in the UV (178 – 210 nm, 210 – 328 nm, 328 – 496 nm), while at the faster speeds (> 9.5 km/s) the radiation is dominated by atomic radiation emitted in the VUV (117 – 153 nm) and the Visible to IR (496 – 888 nm, 888 – 1445 nm).

Table 2. Wavelength ranges used in analysis

Spectral Range	EAST Camera	Dominant Radiators
117 – 153 nm for V $\geq$ 9 km/s	VUV	N, O
123 – 153 nm for V $<$ 9 km/s	VUV	N, O
170 – 178 nm	VUV	N
178 – 210 nm	VUV/UV	NO
210 – 328 nm	UV	N_2, N_2^+, N
328 – 496 nm	UV	N_2^+, N, N_2
496 – 888 nm	Vis/NIR	N, O, N_2
888 – 1445 nm	IR	N, O

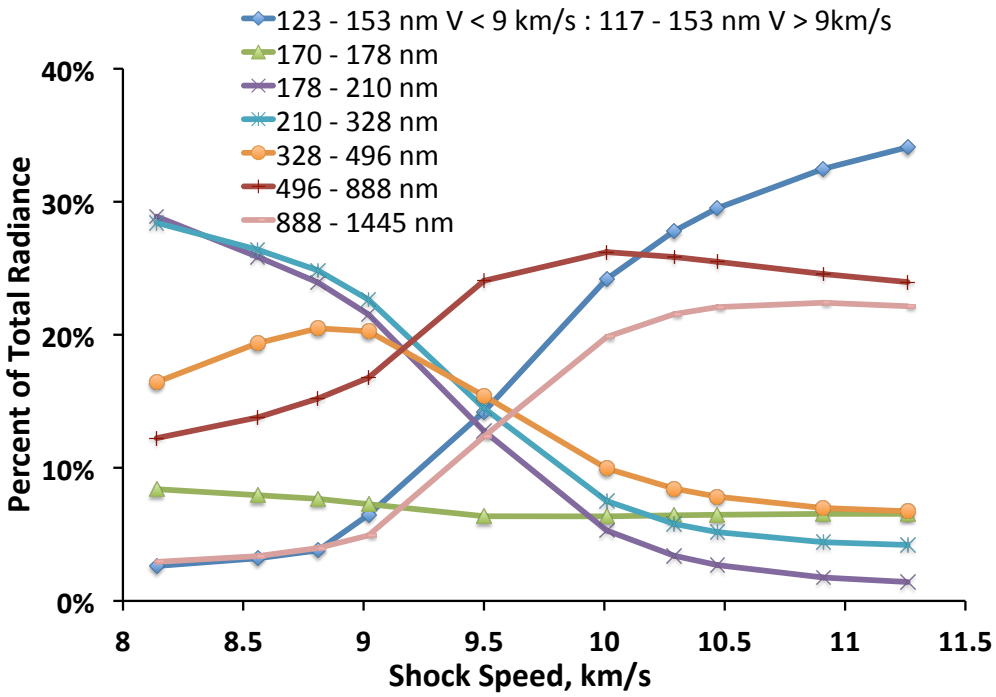

Figure 3. Percentage of radiance emitted from various spectral regions as calculated by HARA.

V. Results

V.A. Simulations vs EAST

Using data from EAST tests 50 and 57, the absolute non-equilibrium metric is computed for the spectral regions listed in Table 2 and shown as a function of shock velocity in Figs. 4 – 7, with lines of best fit created.[3] The same methodology was applied to results from LAURA/HARA, LAURA/NEQAIR and DPLR/NEQAIR simulations. The results from these analyses is displayed in the same way for each spectral region as shown in Figs. 4 – 7. The first and second figures in each set show the absolute non-equilibrium metric comparisons between EAST and the simulations on both linear and log scales. The third plot shows the scatter of the EAST data around the line of best fit. The standard deviation of the scatter is calculated and is used to estimate the uncertainty in the level of agreement between the EAST data and simulations. The standard deviation is shown in the figures as error bars on the line of best fit through the EAST data. Summing the standard deviation over all spectral regions, weighted by the relative radiance measured in EAST for that specific region vs the total radiance measured, provides an indication of the scatter in the EAST data for non-equilibrium. This calculation resulted in a one standard deviation scatter of 31%. Finally, the weighted discrepancy for each spectral range is shown. The "Simulation - EAST Discrepancy" line represents the difference between either the LAURA/HARA or DPLR/NEQAIR simulations and the line of best fit through the experimental data divided by the simulation result. The "Radiance Weighting" line represents the contribution of that individual spectral region as a percentage of the total radiance emitted. The final result for each wavelength region is the "Weighted Discrepancy" line which is the relative difference between the simulation and experiment multiplied by the percentage of contribution for that individual spectral region compared to the total radiance emitted, i.e. the "Simulation - EAST Discrepancy" line multiplied by the "Radiance Weighting" line.

Multiple scenarios are investigated when comparing the experimental data to the computed results; LAURA/HARA, LAURA/NEQAIR and DPLR/NEQAIR. The DPLR/NEQAIR simulations also have results from different chemistries, Park 90 and Park 93, and different electron impact nitrogen excitation rates from either Huo[26] (listed as "Huo N" in all figures) or Park[20] (listed as "Park N" in all figures). The NEQAIR simulations based on flowfields calculated with LAURA use the excitation rates of Huo.[26] HARA uses electronic impact excitation rates for nitrogen compiled by Johnston et al,[11,12] which include rates by Frost.[36] These combinations of calculations will help deduce whether differences between simulations and experiment are due to flowfield issues (e.g. reaction rates, vibration-electron energy relaxation) or radiation modeling issues (non-Boltzmann modeling, spectral databases, excitation rates).

Radiance from atomic nitrogen and oxygen dominate the VUV spectral region from 117 to 153 nm, save for at lower shock speeds where trace amounts of N_2 and NO contribute. Figure 4 shows that there is generally a significant under-prediction for all models and shock speeds. LAURA/HARA under-predicts by as much as 150% around 9 km/s, with an improving level of agreement with increasing shock speed, plateauing at approximately -80% from 10 km/s and above. The DPLR/NEQAIR solutions show a similar plateau level at the higher shock speeds, but very different results for lower shock speeds. Given the substantial difference between the two DPLR/NEQAIR simulations and the differences between LAURA/HARA and LAURA/NEQAIR, it is clear that these solutions are very sensitive to the flowfield, the electronic impact excitation rates, and the non-Boltzmann modeling. The weighted difference between EAST and all models is within 12% at 9 km/s and then heads toward an under-prediction of approximately 32% for the higher shock speeds. The reason for the greater under-prediction is predominantly due to the increasing contribution from the VUV to the total radiance at faster velocities. This under-prediction in the VUV should be the focus of future experiments and model validation/improvements.

In the UV spectral region, 328 to 496 nm, N_2^+ first negative dominates, with small amounts of atomic and molecular nitrogen depending on the shock speed. There is a significant under-prediction of approximately 30% to 50% at 9 km/s, see Fig. 5. The level of agreement between EAST and LAURA/HARA monotonically improves with shock speed until approximately 10 km/s, after which there is excellent agreement with experiment (within 6%). This is likely due to the flow being closer to equilibrium at higher shock speeds when the flow will equilibrate within the 2 cm used in the non-equilibrium metric. Conversely, the DPLR/NEQAIR solutions show an over-prediction of approximately 20%. Due to the region being dominated by N_2^+ first negative, there is no significant dependence on the choice of electron impact nitrogen excitation rate. Furthermore, as the LAURA/HARA and LAURA/NEQAIR solutions give quite different answers between 8.5 and 10.5 km/s, it can be established that in this wavelength range the non-Boltzmann modeling of N_2^+ first

negative in the radiation code is one of the most sensitive parameters. Even though the LAURA/NEQAIR results show an over-prediction between 8.5 and 10 km/s, overall both LAURA/HARA and DPLR/NEQAIR show excellent levels of agreement with the EAST data for the UV spectral region.

The Vis/NIR spectral region of 496 to 888 nm is dominated by atomic oxygen and nitrogen, as well as N_2 (in particular the 1st Positive transition) for the lower shock speed range. Figure 6 shows that for shock speeds from 8 to approximately 9.5 km/s, there is a substantial difference between all the models. This suggests that the results are sensitive to the electron impact excitation rates, the radiation model for N_2 1st Positive, and the flowfield generated by CFD. The level of agreement with LAURA/HARA and DPLR/NEQAIR with the electron impact excitation rates of Park[20] is very good compared to EAST. However, when NEQAIR is run with the electron impact excitation rates of Huo,[26] there is a significant under-prediction of the EAST results at lower speed, by as much as 310%.

The IR spectral region of 888 to 1445 nm is dominated by atomic oxygen and nitrogen. Figure 7 shows that all models over-predict the EAST result from 8 to 9 km/s, this is particularly true for the DPLR/NEQAIR calculations with combinations of either Park 90 and Huo[26] excitation rates or Park 93 and Park[20] excitation rates. The other two models agree within approximately 25%. However, there is significant scatter in both the experimental data and the simulations at these lower speed conditions. Due to the differences in the simulations, as shown in Fig. 7, it can be concluded that the radiance is very sensitive to the choice of electron impact excitation rates. The maximum discrepancy of -200% occurs at 9.5 km/s with faster velocities showing improved agreement. This largest discrepancy is potentially due to the lack of EAST data around 9.5 km/s, and therefore may be a function of an ill-formed fit. Furthermore, any error in the level of ionization calculated by CFD, as it is a critical parameter in the non-Boltzmann model, could also contribute to this discrepancy. Although this peak discrepancy is very high, it occurs at a shock speed where the radiation is relatively low in this wavelength range, see 7(a). For faster speeds, all models agree within approximately 50%.

From the comparisons between DPLR/NEQAIR and EAST, the results indicate that better agreement is achieved with the electron impact excitation rates of Park[20] for the VUV through to Vis/NIR spectral regions, while the rates of Huo[26] provide better agreement in the IR. The rates of Huo[26] should be of higher fidelity as they are based on ab initio calculations, so its unlikely that the rates of Park[20] would be more accurate for states contributing to the emission in the VUV through Red. As such, the poor level of agreement obtained with the Huo[26] excitation rates may be due to the way the different energy levels are grouped together in NEQAIR's non-Boltzmann formulation or might be due to the fact that many aspects of the radiation model have been tuned to match specific experiments or flight data while using the excitation rates of Park.

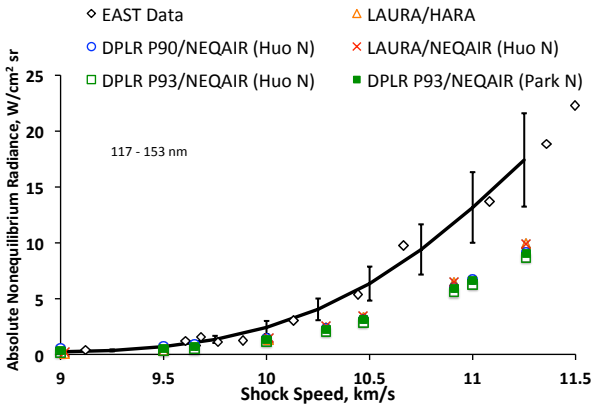

(a) Linear scale

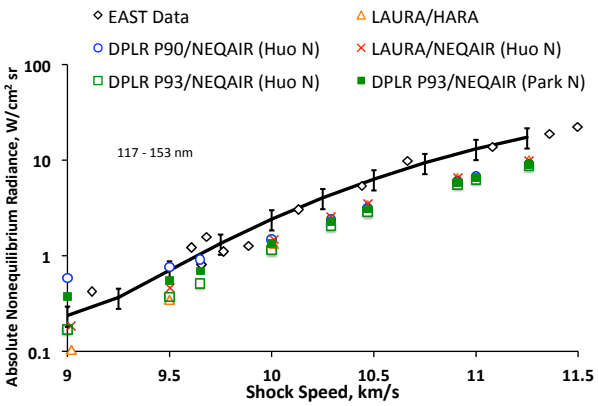

(b) Log scale

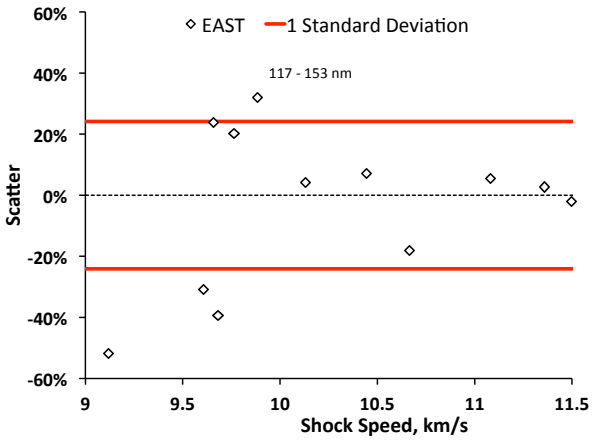

(c) EAST Scatter

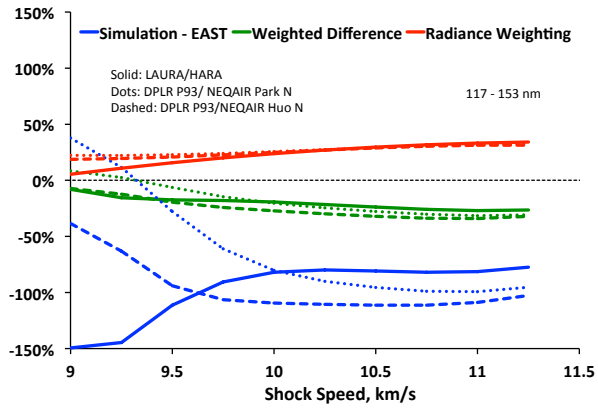

(d) Weighted Discrepancy

Figure 4. Comparison of EAST, NEQAIR and HARA for the 117 to 153 nm spectral region using the absolute non-equilibrium metric.

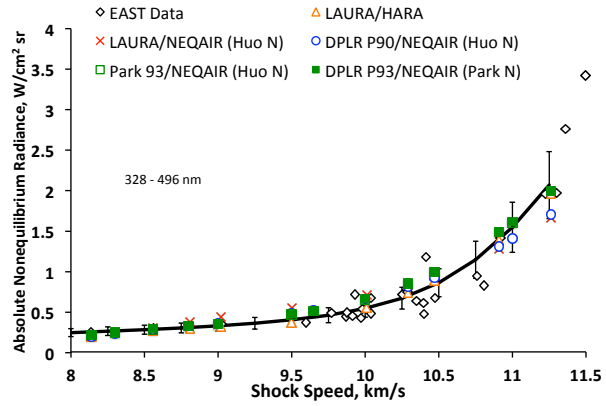

(a) EAST vs HARA linear scale

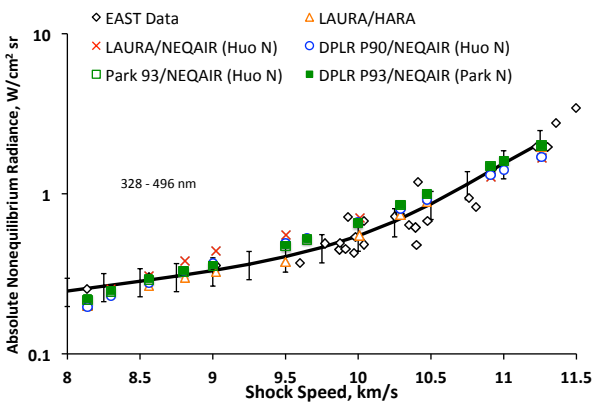

(b) EAST vs HARA log scale

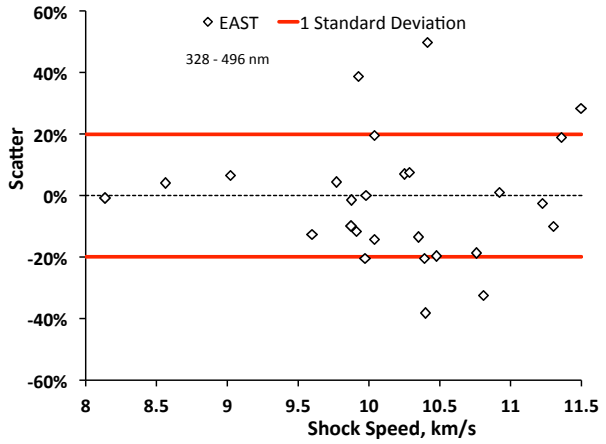

(c) EAST Scatter

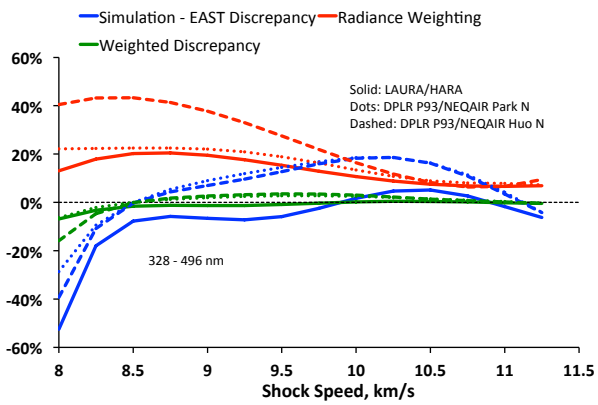

(d) Overall Trend Summation

Figure 5. Comparison of EAST, NEQAIR and HARA for the 328 to 496 nm spectral region using the absolute non-equilibrium metric.

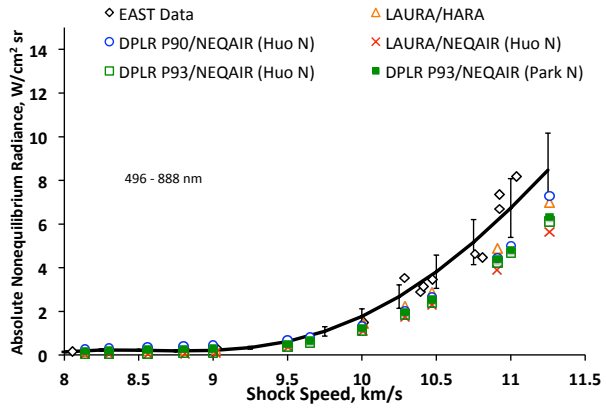

(a) EAST vs HARA linear scale

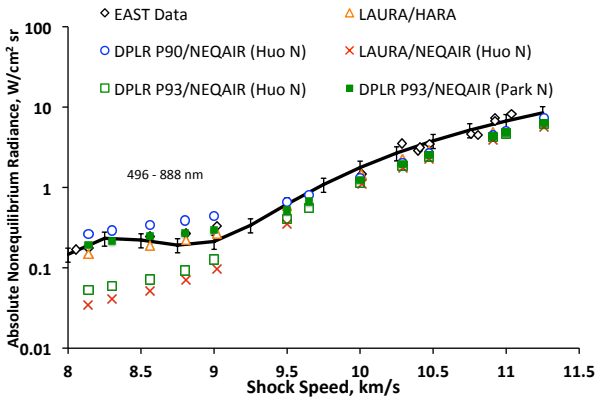

(b) EAST vs HARA log scale

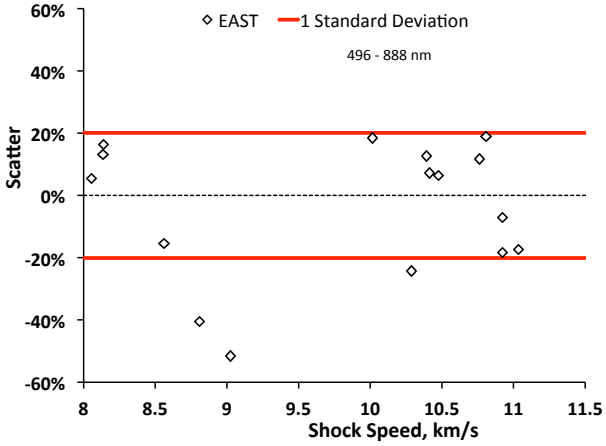

(c) EAST Scatter

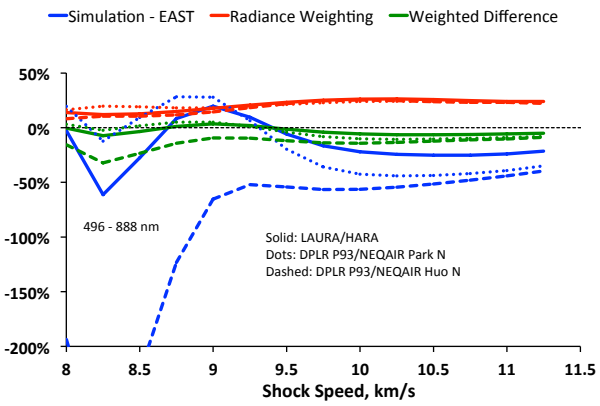

(d) Overall Trend Summation

Figure 6. Comparison of EAST, NEQAIR and HARA for the 496 to 888 nm spectral region using the absolute non-equilibrium metric.

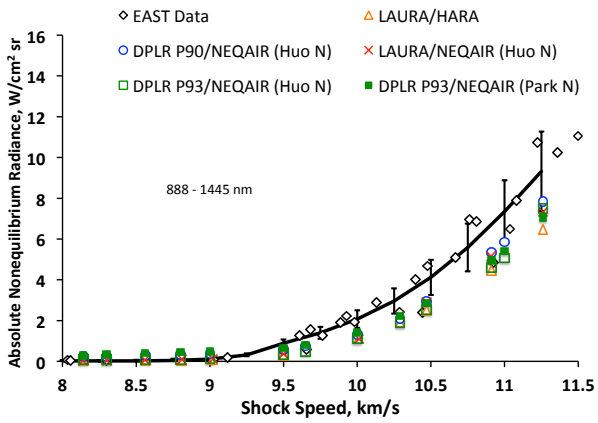

(a) EAST vs HARA linear scale

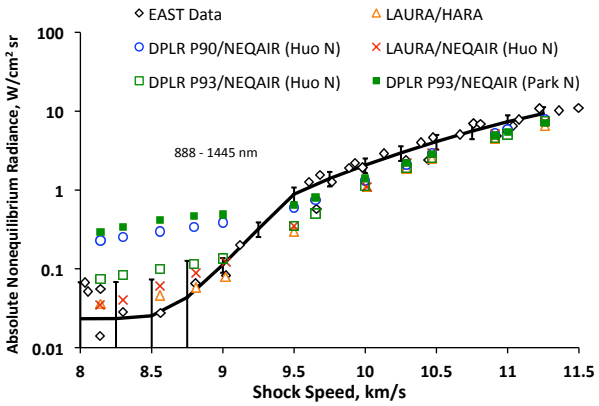

(b) EAST vs HARA log scale

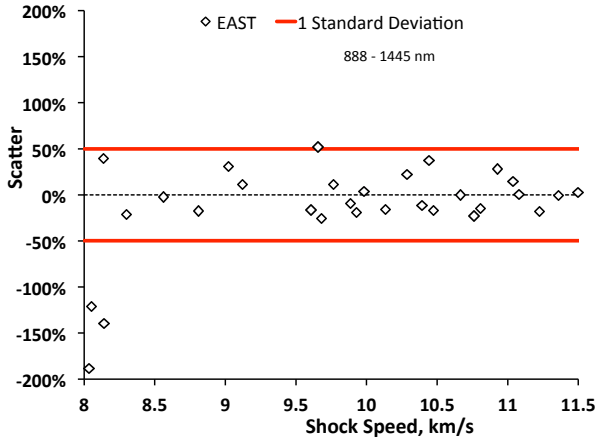

(c) EAST Scatter

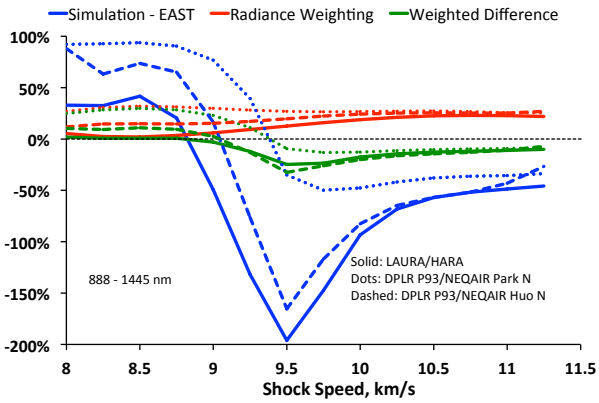

(d) Overall Trend Summation

Figure 7. Comparison of EAST, NEQAIR and HARA for the 888 to 1445 nm spectral region using the absolute non-equilibrium metric.

V.B. NO Non-Boltzmann Update

The 178 to 210 nm spectral range, as shown in Fig. 8, is dominated by emission from NO. Due to the over-prediction between HARA and EAST, the NO model in HARA has been updated by Johnston et al.[16] where the non-Boltzmann rates were tuned to match EAST data from Ref. 2. There is a significant level of scatter in the shots for this wavelength region with the one sigma standard deviation equal to 40%. Even though the NO rates were not specifically tuned to all of the experiments presented in this figure, the updated HARA results are within EAST's one sigma standard deviation error bars. Figure 8 also shows that there is a significant under-prediction of this spectral region by NEQAIR from 8 to 10.5 km/s. Above 10.5 km/s, atomic nitrogen becomes the dominate radiator, and consequently, improved agreement is observed between NEQAIR and EAST. Due to the large scatter in both the shock tube results and the simulations, further experiments and analyses of the NO non-Boltzmann rates are warranted.

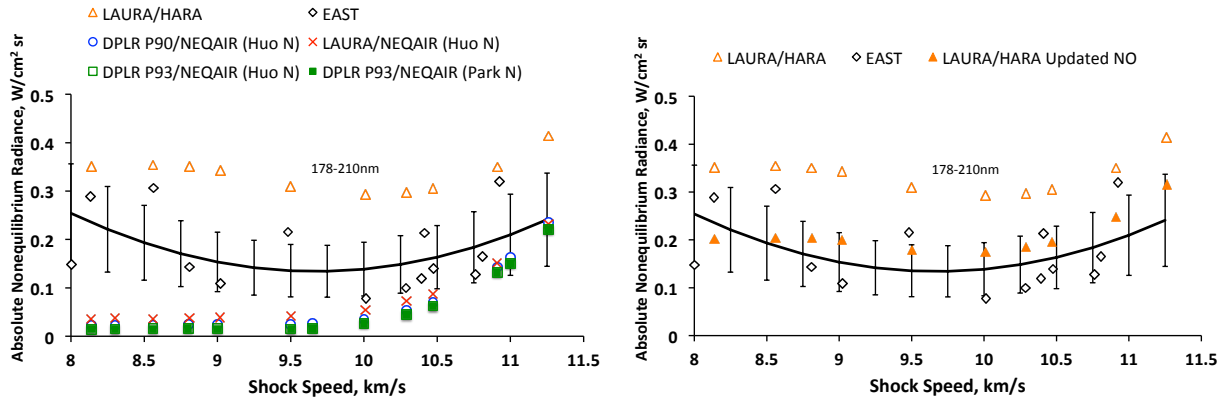

(a) HARA, NEQAIR and EAST Comparisons

(b) Updated NO rates comparison with EAST

Figure 8. Comparison of EAST, NEQAIR and HARA for the 178 to 210 nm spectral region using the absolute non-equilibrium metric.

V.C. Overall Summation

Figure 9 shows the weighted differences between LAURA/HARA and DPLR/NEQAIR simulation results and experimental data for all wavelength regions investigated. At the slowest shock speed conditions, the differences between EAST and LAURA/HARA is within ± 10% for all spectral regions. For the calculations with DPLR/NEQAIR, the discrepancy at lower speed is dominated by two spectral regions, the VUV (178 to 210 nm) and IR (888 to 1445 nm). However, as the VUV is under-predicted and the IR is over-predicted, these differences counter act each other. For the higher speed conditions, the deep VUV spectral region (117 to 153 nm) dominates the differences in all comparisons.

Figure 10(a) shows the summation of these curves, which provide the final overall difference for the simulations compared to EAST. It should be again noted that for these low speed conditions there is no data for the deepest VUV spectral region between 117 and 123 nm. This range is relatively insignificant in terms of radiance at low speed. For the lowest shock speed conditions, less than 9 km/s, the level of agreement is excellent with the solutions obtained with LAURA/HARA and DPLR/NEQAIR with Park 93 and the excitation rates of Park[20] (within 20%). Even though there are significant differences within the spectral breakdown of the discrepancies for these two simulations, the net result is quite similar due to compensating errors. There is, however, a substantial under-prediction at these lower speed conditions when the excitation rates of Huo are used in NEQAIR. The root cause of this under-prediction requires further investigation. Whether it is due to a deficiency in the rates, an issue with the way the lines are grouped in NEQAIR's non-Boltzmann model, or that the result of the incorporation of the Huo[26] excitation rates negatively adjusts the balance and subsequent performance of the reduced-order chemical model, still needs to be determined.

The errors presented in Fig. 10(a) are relative differences, and as such, there is potential for a significant discrepancy to occur at conditions where the impact of radiation to the total heat flux is minimal. Therefore, in Figs. 10(b) and 10(c), an attempt to provide an indication of the absolute magnitude of the differences is provided. The values presented in Figs. 10(b) and 10(c) are the root-sum-square (RSS) of the absolute differences between the simulations and EAST. RSS is used in order to not have compensating errors. This

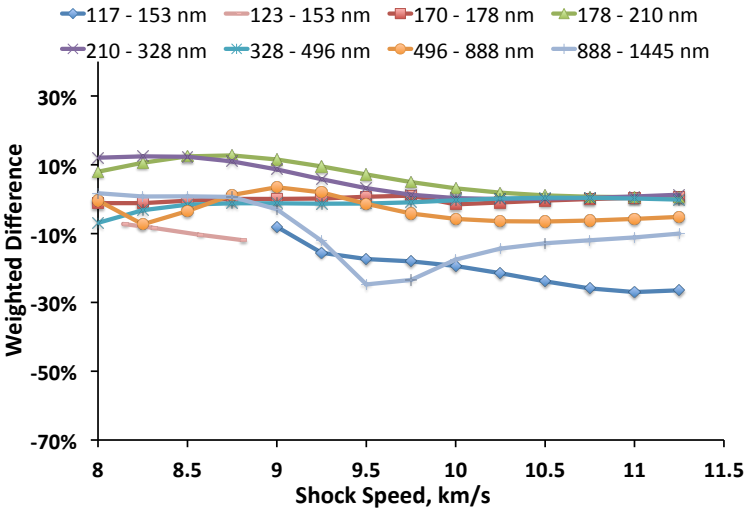

(a) EAST vs LAURA/HARA

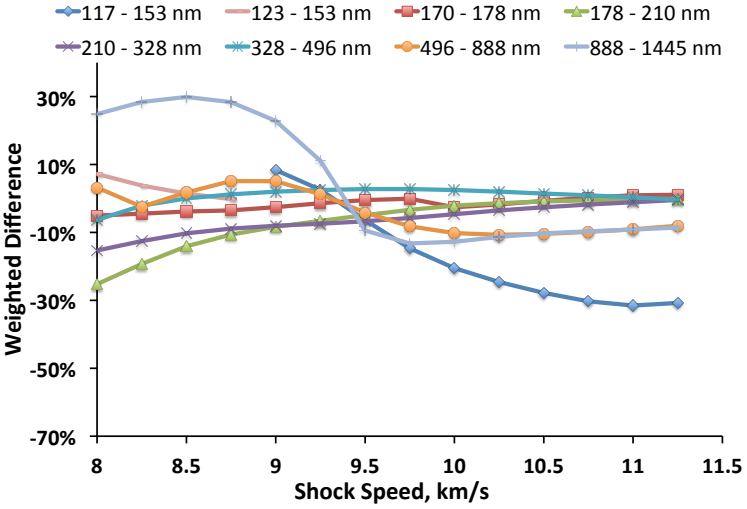

(b) EAST vs DPLR P93/NEQAIR Park N

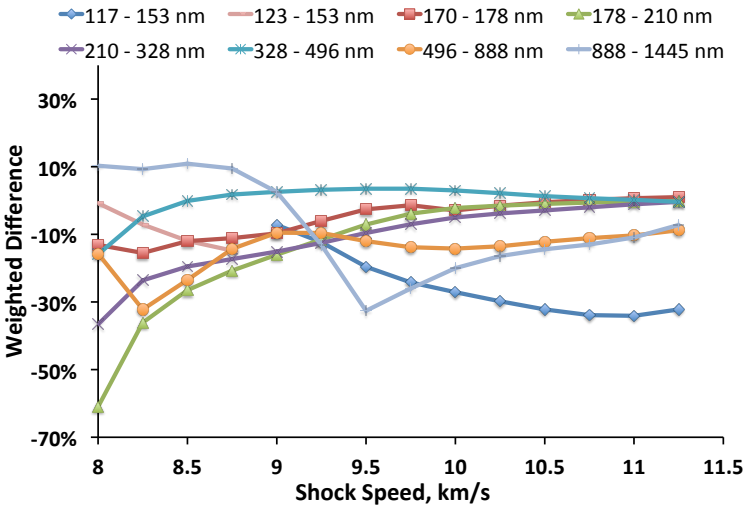

(c) EAST vs DPLR P93/NEQAIR Huo N

Figure 9. Weighted difference between different simulation combinations and EAST.

value corresponds to an estimate of the absolute error in the wall directed radiance between the simulations and EAST for a 2 cm optically thin gas. To convert the radiance into an upper bound for wall directed heat flux, this value is multiplied by 2π. Therefore, at the lower speeds of 8 to 9 km/s, even though there are some large relative differences, the absolute error in radiative heat flux will be less than 1 W/cm^2. At the highest shock speed of 11 km/s, the error will be less than 20 W/cm^2. Table 3 shows the magnitude of these estimated errors in heat flux due to non-equilibrium effects compared to two different entry conditions for both a small (nose radius of 0.5 m) and large (nose radius of 5 m) capsule. The predictions for convective and radiative heating come from the CFD solutions used to create correlations for vehicle heating by Brandis and Johnston.[37] The table shows that the magnitude of the non-equilibrium error in radiative heating can be as high as 12.5% for the conditions shown. However, the magnitude of the non-equilibrium error compared to the total heating is less than 2.5% for all conditions.

Table 3. Magnitude of Error on Heat Flux Due to Non-equilibrium Effects for Various Entry Conditions

Density, kg/m^3	Velocity, km/s	Effective Nose, Radius, m	Convective Heating, Prediction, W/cm^2	Radiative Heating, Prediction, W/cm^2 (% Non-eq. Error)	Total Heating Prediction, W/cm^2 (% Non-eq. Error)
5×10^{-4}	9	0.5	355	8 (12.5%)	363 (0.28%)
5×10^{-4}	11	0.5	610	255 (7.8%)	865 (2.3%)
5×10^{-4}	9	5	111	23 (4.3%)	134 (0.75%)
5×10^{-4}	11	5	180	725 (2.8%)	905 (2.2%)

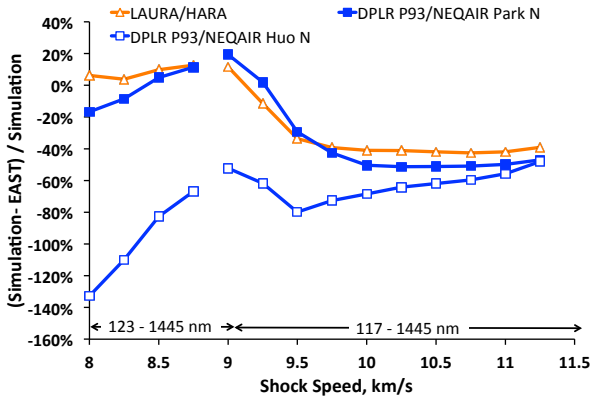

(a) Overall Relative Difference

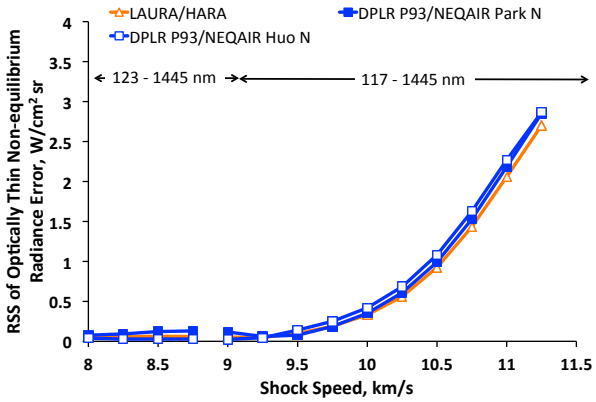

(b) RSS Absolute Difference Linear Scale

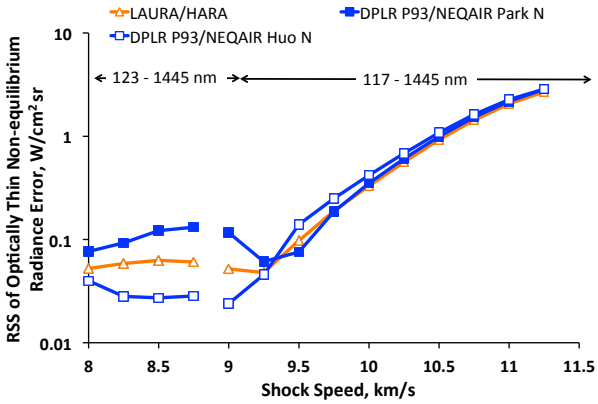

(c) RSS Absolute Difference Log Scale

Figure 10. Overall summation of differences between simulations and EAST.

VI. Conclusion

This paper has analyzed the non-equilibrium portion of Earth re-entry measurements made in the EAST facility. A previously developed non-equilibrium metric has been used to evaluate the level of agreement between the EAST experiments and the code packages LAURA/HARA and DPLR/NEQAIR. The scatter in the EAST results was also analyzed and the one standard deviation scatter was evaluated to be 31%. The results show that the simulations under-predict the experiment by approximately 50% and show an over-prediction of approximately 20% depending on the shock speed. An upper bound estimate for the absolute magnitude of the error due to non-equilibrium effects was evaluated to be 1 W/cm^2 at 9 km/s and 20 W/cm^2 at 11 km/s.

In order to better understand the discrepancies between the two sets of codes, the difference between the reaction rate sets used by each code was examined, and the resulting flowfields analyzed. It became clear by examining the flowfields calculated with Park 90, that the level of ionization calculated was high compared to other chemistry mechanisms, and therefore should not be used in any simulations to predict radiative heating. Calculations were also run with LAURA/NEQAIR to ascertain whether any observed differences were due to the CFD flowfield or the radiation model. The overall differences between simulations with LAURA/HARA and DPLR P93/NEQAIR using the nitrogen electronic excitation rates of Park[20] are in excellent agreement. When the Park[20] excitation rates were swapped out for those of Huo,[26] a substantial under-prediction was observed with respect to EAST. Of particular interest to the under-prediction observed with the rates of Huo,[26] is that if these rates are applied to a backshell case where the flow is expanding, the rates of Huo[26] would provide a substantial over-prediction.

For increased clarity, a breakdown of the comparisons between the simulations and EAST by different spectral regions has been presented. This has highlighted where different spectral regions, and therefore which transitions, need to be the focus of future work. These include spectral regions that are dominated by N_2, N_2^+ and NO as well the observed under-prediction in the VUV. To this extent, an initial comparison was conducted with an updated NO non-Boltzmann model developed in HARA, where improved agreement was observed with EAST. Future analysis between the simulations and EAST should focus on more detailed spatial comparisons of the radiance and comparisons of the spectral radiance. Furthermore, the framework for running radiation calculations for flight cases should be revisited based on the results presented in this paper.

Acknowledgments

The authors would like to thank NASA's Entry Systems Modeling project for their support of this work. Drs Aaron Brandis and Brett Cruden are supported through the NNA15BB15C contract between NASA Ames Research Center and AMA Inc. The authors would like to thank Drs. Joseph Schulz and Michael Barnhardt for helping set up the DPLR solutions. The authors would also like to thank Drs. Joseph Schulz, Grant Palmer and Rich Jaffe for their technical review of this work.

References

[1]Cozmuta, I., Wright, M., Laub, B., and Wilcoxson, W., "Defining Ablative Thermal Protection System Margins for Planetary Entry Vehicles," *42nd AIAA Thermophysics Conference*, Honolulu, HI, 2011, AIAA-2011-3757.

[2]Brandis, A., Johnston, C., Cruden, B., Prabhu, D., and Bose, D., "Uncertainty Analysis and Validation of Radiation Measurements for Earth Re-Entry," *Journal of Thermophysics and Heat Transfer*, Vol. 29, No. 2, 2015, pp. 209–221.

[3]Brandis, A., Johnston, C., Cruden, B., and Prabhu, D., "Validation of High Speed Earth Atmospheric Entry Radiative Heating from 9.5 to 15.5 km/s," *AIAA*, Vol. AIAA 2012-2865, New Orleans, Louisiana, June 2012.

[4]Cruden, B., Martinez, R., Grinstead, J., and Olejniczak, J., "Simultaneous Vacuum-Ultraviolet Through Near-IR Absolute Radiation Measurement with Spatiotemporal Resolution in An Electric Arc Shock Tube," *41st AIAA Thermophysics Conference*, San Antonio, Texas, 2009, AIAA-2009-4240.

[5]Cruden, B., "Absolute Radiation Measurements in Earth and Mars Entry Condition," *Radiation and Gas-Surface Interaction Phenomena in High-Speed Re-Entry*, Vol. Von Karman Institute Lecture Series, 2014.

[6]Cruden, B. and Johnston, C., "Characterization of EFT-1 Radiative Heating and Radiometer Data," *46th AIAA Thermophysics Conference*, Washington, D.C., 2016, AIAA-2016-4113.

[7]Mazaheri, A., Gnoffo, P., Johnston, C., and Kleb, B., "LAURA Users Manual," Tech. Rep. NASA TM 2010-216836, 2010.

[8]Gnoffo, P., Gupta, R., and Shinn, J., "Conservation equations and physical models for hypersonic air flows in thermal and chemical nonequilibrium," Tech. Rep. NASA TP-2867, 1989.

[9]Roe, P., "Approximate Riemann Solvers, Parameter Vectors, and Difference Schemes," *Journal of Computational Physics*, Vol. 43, No. 2, 1981, pp. 357–372.

[10]Yee, H., "On Symmetric and Upwind TVD Schemes," Tech. Rep. NASA TM-88325, 1986.

[11]Johnston, C., Hollis, B., and Sutton, K., "Spectrum Modeling for Air Shock-Layer Radiation at Lunar-Return Conditions," *Journal of Spacecraft and Rockets*, Vol. 45, No. 5, 2008, pp. 865–878.

[12]Johnston, C. O., Hollis, B., and Sutton, K., "Non-Boltzmann Modeling for Air Shock Layers at Lunar Return Conditions," *Journal of Spacecraft and Rockets*, Sep.-Oct. 2008.

[13]Ralchenko, Y., "NIST Atomic Spectra Database, Version 3.1.0," physics.nist.gov/PhysRefData/ASD/, July 2006, last accessed September 3rd, 2007.

[14]The Opacity Project Team, *The Opacity Project*, Vol. 1, Bristol and Philadelphia: Institute of Physics Publishing, 1995.

[15]Cunto, W., Mendoza, C., Ochsenbein, F., and Zeippen, C., "TOPbase at the CDS," *Astronomy and Astrophysics*, Vol. 275, Aug. 1993, pp. L5–L8, see also http://cdsweb.u-strasbg.fr/topbase/topbase.html.

[16]Johnston, C., Brandis, A., and Panesi, M., "Refinements to Afterbody Radiative Heating Simulations for Earth Entry," *46th AIAA Thermophysics Conference*, Washington, D.C., 2016.

[17]Wright, M., *A Family of Data-Parallel Relaxation Methods for the Navier-Stokes Equations*, Ph.D. thesis, University of Minnesota, 1997.

[18]Wright, M., Candler, G., and Bose, D., "Data-Parallel Line Relaxation Method for the Navier-Stokes Equations," *AIAA Journal*, Vol. 36, No. 9, 1998, pp. 1603–1609.

[19]Wright, M., White, T., and Mangini, N., "Data-Parallel Line Relaxation (DPLR) Code User Manual Acadia-Version 4.01.1," NASA/TM-2009-215388, NASA Ames Research Center, October 2009.

[20]Whiting, E., Park, C., Yen, L., Arnold, J., and Paterson, J., "NEQAIR96, Nonequilibrium and Equilibrium Radiative Transport and Spectra Program: User's Manual," Technical Report NASA RP-1389, Ames Research Center, Moffett Field, Moffett Field, 1996.

[21]Kramida, A., Ralchenko, Y., Reader, J., and Team, N. A., "NIST Atomic Spectra Database, Version 5.0.0," physics.nist.gov/asd/, July 2012, last accessed July, 2012.

[22]Tashkun, S. and Perevalov, V., "CDSD-4000: High-Resolution, High-Temperature Carbon Dioxide Spectroscopic Databank," *Journal of Quantitative Spectroscopy and Radiative Transfer*, Vol. 112, No. 9, 2011, pp. 1403–1410.

[23]Cruden, B. and Brandis, A., "Updates to the NEQAIR Radiation Solver," St. Andrews, Scotland, November 2014.

[24]Gilmore, F., Laher, R., and Espy, P., "Franck-Condon factors, r-centroids, electronic transition moments, and Einstein coefficients for many nitrogen and oxygen band systems," *Journal of Physical Chemistry Reference Data*, Vol. 21, 1992, pp. 1005.

[25]Itikawa, Y., "Cross sections for electron collisions with nitrogen molecules," *Journal of Physical Chemistry Reference Data*, Vol. 35, No. 1, 2006, pp. 31–53.

[26]Huo, W., Liu, Y., Panesi, M., Munafo, A., Wray, A., and Carbon, D., "Electron-Impact Excitation Cross Sections for Modeling Non-Equilibrium Gas," *Proceedings of the 53rd AIAA Aerospace Sciences Meeting and Exhibition*, AIAA, Kissimmee, Florida, 2015, AIAA-2015-1896.

[27]Brandis, A., Johnston, C., Cruden, B., and Prabhu, D., "Investigation of Nonequilibrium Radiation for Mars Entry," *51st AIAA Aerospace Sciences Meeting*, Grapevine, Texas, 2013, AIAA-2013-1055.

[28]Park, C., *Nonequilibrium hypersonic aerothermodynamics*, Wiley, New York, 1990.

[29]Park, C., "Review of chemical-kinetic problems for future NASA missions, I. Earth entries," *Journal of Thermophysics and Heat Transfer*, Vol. 7, 1993, pp. 385–398.

[30]Johnston, C., "Study of Aerothermodynamic Modeling Issues Relevant to High-Speed Sample Return Vehicles," *Radiation and Gas-Surface Interaction Phenomena in High-Speed Re-Entry*, Vol. Von Karman Institute Lecture Series, 2014.

[31]Bourdon, A. and Vervisch, P., "Study of a low-pressure nitrogen plasma boundary layer over a metallic plate," *Physics of Plasmas*, Vol. 4, No. 7, 1997, pp. 4144.

[32]Teulet, P., Gonzalez, J., Mercado-Cabrera, A., Cressault, Y., and Gleizes, A., "One-dimensional hydro-kinetic modelling of the decaying arc in air-PA66-copper mixtures: I. Chemical kinetics, thermodynamics, transport and radiative properties," *Journal of Physics D: Applied Physics*, Vol. 42, 2009.

[33]Fujita, K., Yamada, T., and Ishii, N., "Impacts of Ablation Gas Kinetics on Hyperbolic Entry Radiative Heating," *44th AIAA Aerospace Sciences Meeting and Exhibit*, Reno, Nevada, 2006, AIAA-2006-1185.

[34]Bose, D. and Candler, G., "Thermal nonequilibrium rates of the Zeldovich reactions," *AIAA*, Reno, Nevada, January 1997, AIAA 1997-0133.

[35]Cruden, B., "Electron Density Measurement in Re-entry Shocks for Lunar Return," *Journal of Thermophysics and Heat Transfer*, Vol. 26, 2012, pp. 222–230.

[36]Frost, R., Awakowicz, P., Summers, H. P., and Badnell, N., "Calculated Cross Sections and Measured Rate Coefficients for Electron-Impact Excitation of Neutral and Singly Ionized Nitrogen," *Journal of Applied Physics*, Vol. 84, No. 6, 1998, pp. 2989–3003.

[37]Brandis, A. and Johnston, C., "Characterization of Stagnation-Point Heat Flux for Earth Entry," *11th AIAA/ASME Joint Thermophysics and Heat Transfer Conference*, Atlanta, Georgia, 2014, AIAA 2014-2374.